NeuroImage: Clinical 42 (2024) 103600

Contents lists available at ScienceDirect

NeuroImage: Clinical

journal homepage: www.elsevier.com/locate/ynicl

Multi-tracer PET correlation analysis reveals disease-specific patterns in Parkinson's disease and asymptomatic LRRK2 pathogenic variant carriers compared to healthy controls

Julia G. Mannheim [a,b,c,1,*], Jessie Fanglu Fu [a,d,1], Tilman Wegener [a,e], Ivan S. Klyuzhin [f], Nasim Vafai [g], Elham Shahinfard [f,g], Jessamyn McKenzie [g], Audrey Strongosky [i], Zbigniew K. Wszolek [i], A. Jon Stoessl [f,h], Vesna Sossi [a,h]

[a] Department of Physics and Astronomy, University of British Columbia, Vancouver, BC, Canada
[b] Werner Siemens Imaging Center, Department of Preclinical Imaging and Radiopharmacy, Eberhard-Karls University Tuebingen, Tuebingen, Germany
[c] Cluster of Excellence iFIT (EXC 2180) "Image Guided and Functionally Instructed Tumor Therapies", University of Tuebingen, Tuebingen, Germany
[d] Athinoula A. Martinos Center for Biomedical Imaging, Department of Radiology, Massachusetts General Hospital, Charlestown, MA, United States
[e] Department of Medical Engineering, University of Luebeck, Luebeck, Germany
[f] Division of Neurology, Department of Medicine, University of British Columbia, Vancouver, BC, Canada
[g] Pacific Parkinson's Research Centre, The University of British Columbia, Vancouver, British Columbia, Canada
[h] Djavad Mowafaghian Centre for Brain Health, Pacific Parkinson's Research Centre, University of British Columbia & Vancouver Coastal Health, Vancouver, BC, Canada
[i] Mayo Clinic Florida, Department of Neurology, Jacksonville, FL, USA

ARTICLE INFO

Keywords:
Joint pattern analysis
PET
PD
LRRK2
HCs

ABSTRACT

Several genetic pathogenic variants increase the risk of Parkinson's disease (PD) with pathogenic variants in the leucine-rich repeat kinase 2 (LRRK2) gene being among the most common. A joint pattern analysis based on multi-set canonical correlation analysis (MCCA) was utilized to extract PD and LRRK2 pathogenic variant-specific spatial patterns in relation to healthy controls (HCs) from multi-tracer Positron Emission Tomography (PET) data. Spatial patterns were extracted for individual subject cohorts, as well as for pooled subject cohorts, to explore whether complementary spatial patterns of dopaminergic denervation are different in the asymptomatic and symptomatic stages of PD. The MCCA results are also compared to the traditional univariate analysis, which serves as a reference.

We identified PD-induced spatial distribution alterations common to DAT and VMAT2 in both asymptomatic LRRK2 pathogenic variant carriers and PD subjects. The inclusion of HCs in the analysis demonstrated that the dominant common PD-induced pattern is related to an overall dopaminergic terminal density denervation, followed by asymmetry and rostro-caudal gradient with deficits in the less affected side still being the best marker of disease progression.

The analysis was able to capture a trend towards PD-related patterns in the LRRK2 pathogenic variant carrier cohort with increasing age in line with the known increased risk of this patient cohort to develop PD as they age. The advantage of this method thus resides in its ability to identify not only regional differences in tracer binding between groups, but also common disease-related alterations in the spatial distribution patterns of tracer binding, thus potentially capturing more complex aspects of disease induced alterations.

1. Introduction

Parkinson's disease (PD) is the second most common neurodegenerative disorder, characterized by the loss of dopaminergic neurons in the substantia nigra *pars compacta* projecting to the striatal regions (Stoessl, 2011). Clinical manifestations of PD include resting

* Corresponding author at: Werner Siemens Imaging Center, Department of Preclinical Imaging and Radiopharmacy, Eberhard-Karls University Tuebingen, Tuebingen, Germany.
E-mail address: julia.mannheim@med.uni-tuebingen.de (J.G. Mannheim).
[1] Authors contributed equally to the work.

https://doi.org/10.1016/j.nicl.2024.103600
Received 29 September 2023; Received in revised form 6 March 2024; Accepted 31 March 2024
Available online 1 April 2024

tremor, bradykinesia, rigidity and postural instability (Stoessl, 2011; Antony, 2013). Motor manifestations of PD typically appear when approximately 30–50 % of the dopaminergic neurons are lost. Dopaminergic denervation occurs first in the dorsal posterior putamen contralateral to the more affected body side, while the ventral and anterior putamen, as well as the caudate nucleus, remain relatively spared in early disease (Stoessl, 2011).

It is now widely recognized that several genetic pathogenic variants increase the risk of PD with pathogenic variants in the leucine-rich repeat kinase 2 (LRRK2) gene being among the most common (Tolosa, 2020; Taymans and Greggio, 2016). LRRK2 pathogenic variants typically result in increased kinase activity, which increases cytotoxicity in cultured neurons, and is thus being investigated as a potential therapeutic target (Taymans and Greggio, 2016). LRRK2-related PD (Tolosa, 2020; Rui, 2018; Wile, 2017) usually appears as late-onset PD with clinical features and therapeutic response very similar to idiopathic PD (Tolosa, 2020). Given the incomplete penetrance of LRRK2 pathogenic variants, it would be beneficial to identify asymptomatic LRRK2 pathogenic variant carriers who are at particularly high risk of developing PD together with an estimate of when disease is likely to occur. Such knowledge would allow insights into preclinical disease and disease triggering mechanisms; multiple studies are focusing on developing novel biomarkers for this purpose (Tolosa, 2020).

Functional imaging with Positron Emission Tomography (PET) has been utilized over the past decades to determine PD-related neurodegeneration patterns, mostly targeting different aspects of the dopaminergic system. [^{11}C]dihydrotetrabenazine ([^{11}C]DTBZ) assesses the vesicular monoamine transporter 2 (VMAT2) and can be used as a measure of monoaminergic nerve terminal density, while dopamine transporter (DAT) markers such as [^{11}C]methylphenidate ([^{11}C]MP) and a large number of ^{11}C- and ^{18}F-labeled tropane derivatives can be used to study the density of synaptic dopamine reuptake machinery (Stoessl, 2011; Peng, 2013).

While traditional PET data analysis approaches rely on univariate analysis methods, we recently demonstrated the advantage of a joint pattern analysis based on multi-set canonical correlation analysis (MCCA) to extract complementary dopaminergic denervation patterns from multi-tracer PET in PD (Fu, 2019). MCCA was shown to capture disease-associated alterations with higher sensitivity compared to traditional univariate analysis approaches, as it synergistically combined information from more than one imaging target. Three orthogonal common spatial patterns were extracted for PD subjects scanned with both [^{11}C]DTBZ and [^{11}C]MP, reflecting complementary disease-related information about VMAT2 and DAT: (i) asymmetry between the more and less affected striatal regions, (ii) a denervation gradient with the most preserved tracer uptake in the caudate nucleus and lowest uptake in the posterior putamen and (iii) progressive denervation pattern in the less affected striatum compared to the more affected striatum – likely reflecting a floor effect in the latter; the expression of this pattern showed stronger correlation with disease duration for both DTBZ and MP compared to univariate measures (i.e. uptake in individual substriatal regions). While this study captured patterns most relevant within early established PD (disease duration 4.67 ± 2.83 years), a spatial pattern specific to the preclinical stage could not be reliably established due to the lack of control and at-risk (e.g. asymptomatic LRRK2 pathogenic variant carriers) groups.

The present study extends the MCCA analysis to extract PD and LRRK2 pathogenic variant-specific spatial patterns in relation to healthy controls (HCs). Spatial patterns were extracted for individual subject cohorts, as well as for pooled subject cohorts, to explore whether complementary spatial patterns of dopaminergic denervation are different in the asymptomatic and symptomatic stages of PD. The MCCA results are also compared to the traditional univariate analysis, which serves as a reference. Given the increased risk of PD in the presence of pathogenic LRRK2 variants (Wile, 2017), we speculate that the identification of a dopaminergic denervation pattern in this subject group might reveal specific alterations reflective of either incipient disease or risk factors.

2. Material and methods

2.1. Study participants

Three subject cohorts consisting of participants from previous studies performed in our centre (Nandhagopal, 2009; Adams, 2005; Sossi, 2010) were included in this study: HC (n = 27, 16 female, 11 male), asymptomatic LRRK2 pathogenic variant carriers (n = 11, 6 female, 5 male) and sporadic PD (n = 40, 11 female, 29 male, disease duration estimated from the onset of symptoms reported by the subjects: 7.5 ± 5.9 y). All HC and PD subjects were right-handed to limit potential handedness-related confounds. Due to the relatively low number of asymptomatic LRRK2 pathogenic variant carriers, both left- (n = 3) and right-handed (n = 8) subjects were included; no significant difference in the average dominant and non-dominant putaminal side of the non-displaceable binding potential (BP_{ND}) values between left- and right-handed subjects were detected for the asymptomatic LRRK2 pathogenic variant carriers. Motor dysfunction was clinically staged using the Hoehn and Yahr scale in the off-medication (minimum 12 h) state. Table 1 lists a detailed overview of study participants and corresponding clinical characteristics. The study was approved by the Clinical Research Ethics Board of the University of British Columbia and all subjects provided written informed consent.

2.2. Scanning protocols

All study subjects underwent DTBZ and MP PET scans performed on the ECAT 953B/31 tomograph (CTI Systems, Siemens, Knoxville, TN, USA) in 3D mode with a spatial resolution of ~ (8 mm)^3 at the center of the field of view (Sossi, 1998). Positioning of the subjects was performed using external lasers aligning the gantry with the inferior orbital-external meatal line. To minimize head movements, custom-fitted thermoplastic masks were applied. Intravenous tracer injection (DTBZ: 202.7 ± 32.4 MBq; MP: 198.9 ± 26.3 MBq) was performed over 60 s using an infusion pump (Harvard Apparatus, Holliston, MA, USA). ^{11}C-PET scans were performed sequentially and were separated by at least 2.5 h to allow for tracer decay and to avoid any interferences. PET acquisition was performed for 60 min, data were histogrammed into 16

Table 1
Clinical characteristics of all three patient cohorts.

	healthy controls (n = 27)	asymptomatic LRRK2 pathogenic variant carriers (n = 11)	sporadic PD (n = 40)
gender (m/f)	11/16	5/6	29/11
age (years)	56.6 ± 12.3	52.9 ± 16.4	62.2 ± 10.5
disease duration (years)	N/A	N/A	7.5 ± 5.9
Hoehn and Yahr scale	N/A	0.3 ± 0.9	1.7 ± 0.5
gene pathogenic variant	N/A	R1411C (n = 6), G2019S (n = 3), Y1699C (n = 2)	N/A
asymmetry index putamen [%]	7.78 ± 6.58	6.31 ± 2.05	23.24 ± 14.35

Data are presented as mean ± standard deviation. Disease duration is estimated from the time of symptoms onsets as reported by the subjects. PD = Parkinson's Disease; LRRK2 = leucine-rich repeat kinase 2. N/A: not applicable.

frames (4x1 min, 3x2 min, 8x5 min, 1x10 min) and reconstructed using a filtered backprojection (FBP) algorithm with a matrix of 128 x 128 x 31 resulting in a reconstructed voxel size of 2.6078 x 2.6078 x 3.375 mm^3. Transmission data acquired with external ^{68}Ge rods were used to correct for attenuation. Data were corrected for scatter, detector normalization and attenuation.

2.3. Image processing and analysis

Reconstructed dynamic PET sequences were frame-to-frame realigned based on a rigid-body transformation (Statistical Parametric Mapping (SPM), version 12, Wellcome Trust Centre for Neuroimaging, University College London, UK) to minimize the effect of motion during the scan; the mean over time PET image of each subject was calculated. Tracer-specific PET templates were calculated in the ECAT space by co-registering the mean images of healthy control subjects using rigid-body transformation. Templates were resized and co-registered to match the dimensions of a Montreal Neurological Institute (MNI) MR template (292 x 193 x 193, voxel size 1 x 1 x 1 mm^3) using a combination of manual, rigid and non-linear registration approaches. All PET scans were subsequently co-registered to the tracer-specific PET template in ECAT space using rigid and non-linear registration. Parametric BP_{ND} maps were calculated in the ECAT space using the two-step simplified reference tissue model (SRTM2 (Wu and Carson, 2002) with the occipital cortex as reference region. Parametric BP_{ND} maps were resized and co-registered to the MNI space by using the transformation matrix between the tracer-specific template and the MNI space. Circular regions of interest (ROIs, size 1105 mm^3) were manually placed bilaterally in the MNI space on 17 axial slices: one ROI for caudate and three covering the full length of the putamen (putamen 1: anterior, putamen 2: middle, putamen 3: posterior). Registration quality and ROI position were visually checked for each scan by an observer blind to the analysis outcomes. Mean over slices BP_{ND} values of the 8 ROIs were determined for the less and more affected sides for PD (determined based on the mean DTBZ BP_{ND} in the putamen), and for the dominant and non-dominant sides for HCs and asymptomatic LRRK2 pathogenic variant carriers.

2.4. Univariate analysis

Traditional univariate analysis was performed as a reference for the outcomes of the MCCA analysis and to ensure general consistency with previously published results (Wile, 2017; Sossi, 2010; Nandhagopal, 2011). Since no difference in BP_{ND} values between the dominant and non-dominant side was found for the HC and no lateral asymmetry was found for the asymptomatic LRRK2 pathogenic variant carriers (asymmetry index of putamen <10 %, respectively, following the calculation from Zijlmans et al. (Zijlmans, 2007), see Table 1), the BP_{ND} values for both hemispheres were averaged for these subjects. Then, the differences between the average putaminal BP_{ND} values of HCs and asymptomatic LRRK2 pathogenic variant carriers and the BP_{ND} values of the less and more affected side of the PD subjects were examined by performing two-sample t-tests. Statistical significance level was set to $p < 0.05$ after Bonferroni-Holm's correction for multiple comparisons.

Linear correlation analyses between BP_{ND} values averaged over both sides of the putamen and age were performed separately for DTBZ and MP for HCs and asymptomatic LRRK2 pathogenic variant carriers. Multiple regression analyses between DTBZ and MP BP_{ND} values and disease duration and age as variables were performed for the less and more affected putamen for the PD subjects. Statistical significance level was set to $p < 0.05$ without correction for multiple comparisons.

2.5. Joint pattern analysis

A joint pattern analysis approach based on MCCA has been previously described in detail by Fu et al. (Fu, 2019). In brief, the reported data-driven analysis approach is based on identifying common spatial information among datasets obtained with each tracer by maximizing the correlation between the subject expressions of spatial patterns. Before undergoing MCCA, data (ROI-based BP_{ND} values for each subject) are demeaned and whitened, which serves to scale the values to a mean of zero with equal variance and reduces the number of ROI-based BP_{ND} to a lower number of linearly independent combinations. These data are then linearly transformed once more under the constraint that subjects' expression of the patterns of each tracer are maximally correlated, which yields canonical variates. Spatial loadings determine the contribution of each demeaned ROI's BP_{ND} to each component. Subject scores for each component (canonical variate) determine the strength of the expression of that particular spatial pattern for that subject.

The resulting canonical variates are ordered in order of decreasing correlation strengths between the subjects' expressions of the DTBZ and MP spatial patterns. The identified spatial patterns are by construct orthogonal and thus reflecting distinct mechanisms independent of one another.

The joint pattern analysis approach was applied to the BP_{ND} values in either a single subject group or a combination of subject groups:

(i) HCs only,
(ii) asymptomatic LRRK2 pathogenic variant carriers only,
(iii) PD subjects only, and
(iv) HCs pooled with asymptomatic LRRK2 pathogenic variant carriers and PD subjects.

The number of canonical variates was set to three for all subject groups. For (i) to (iii), spatial patterns were determined separately to detect cohort-specific spatial patterns. Note that in this case data are demeaned within each group separately. Spatial patterns of pooled cohorts were determined by pooling the less and more affected side of PD subjects with the mean BP_{ND} of HCs and/or asymptomatic LRRK2 pathogenic variant carriers, respectively. In this case data are demeaned using the data from all three groups. The spatial patterns of pooled cohorts are expected to reveal information related to risk factor-associated alterations related to LRRK2 pathogenic variants and/or disease-progression in pre-symptomatic and symptomatic stages of PD by identifying main variations between the cohorts. Note that when the HC and/or the LRKK2 subjects' data are pooled with the PD group, we distinguish between the less affected and more affected striatal regions for the PD cohort and use the average BP_{ND} values between the dominant and non-dominant side for the HC and LRRK2 pathogenic variant carriers. Statistical significance of the extracted canonical variates was examined with repeated random permutation test. Statistical significance level of MCCA loadings was set to $p < 0.05$ after Bonferroni-Holm's correction for multiple comparisons.

Results for HCs pooled with asymptomatic LRRK2 pathogenic variant carriers, HCs pooled with PD subjects and asymptomatic LRRK2 pathogenic variant carriers pooled with PD subjects can be found in the supplementary data.

For each of the cohorts, the subject scores along each canonical variate pair were utilized to quantify the expressions of the spatial patterns for each subject. Linear correlation analyses were performed between the subject scores and age for HCs and asymptomatic LRRK2 pathogenic variant carriers. A multiple regression analysis between the subject scores and age and disease duration was performed for the PD subjects. Two-sample t-tests were performed to determine statistically relevant group separations between the subject scores obtained in the analysis of the pooled cohorts. The statistical significance level of the correlation between subject scores with age and/or disease duration and the group differences was set to $p < 0.05$ without correction for multiple comparisons. The correlation strength (R^2) between DTBZ and MP subject scores along each canonical variate was calculated for each individual and pooled cohort analysis to estimate the level of commonality between the spatial patterns extracted from the two imaging targets. A

higher level of correlation in the PD cohort compared to the HC was taken to be indicative of a disease-related relationship.

3. Results

3.1. Univariate analysis

No significant difference in age between subject cohorts was found.

Average putaminal BP_{ND} values of HCs and asymptomatic LRRK2 pathogenic variant carriers were significantly higher ($p < 0.0001$) compared to the less and more affected side of the putamen of the PD subjects for both tracers (Fig. 1, supplementary Table 1). Averaged putaminal BP_{ND} values of the HCs were significantly higher compared to asymptomatic LRRK2 pathogenic variant carriers for both tracers (DTBZ: $p = 0.0005$, MP: $p = 0.004$). Less and more affected putaminal BP_{ND} values were significantly different for PD subjects for both tracers ($p < 0.01$).

For the HCs, correlation analysis revealed significant inverse correlation of average putaminal BP_{ND} with age (Fig. 2a, supplementary Table 2) for MP ($p = 0.0002$), whereas no correlation was detected for DTBZ. A similar correlation was detected for asymptomatic LRRK2 pathogenic variant carriers with significant inverse correlation of BP_{ND} with age for MP ($p = 0.0008$, Fig. 2b).

Multiple regression analysis of the BP_{ND} of PD subjects demonstrated significant correlation with disease duration as the sole explanatory variable in the less affected side of the putamen for both tracers (Fig. 2c, supplementary Table 2, DTBZ: $p = 0.008$, MP: $p = 0.0007$). The more affected putaminal side of PD subjects revealed a significant correlation with disease duration for DTBZ (Fig. 2d, $p = 0.03$) and a borderline significant correlation for MP ($p = 0.05$). The BP_{ND} in the less and more affected putamen of one PD subject (disease duration: 10 y, age: 60.2 y) appeared as outlier for both tracers with uptake values more than 3 standard deviations higher compared to the BP_{ND} values of the PD group and within the HC range.

3.2. Joint pattern analysis

To limit the number of comparisons, we focus here on the joint pattern analysis of individual cohorts of HCs, asymptomatic LRRK2 pathogenic variant carriers and PD subjects, as well as on the pooled analysis of all three cohorts. Additional analyses focusing on the pooled cohorts of HCs & asymptomatic LRRK2 pathogenic variant carriers, HCs & PD subjects, and asymptomatic LRRK2 pathogenic variant carriers & PD subjects can be found in the supplementary information.

3.2.1. Individual cohorts

Healthy controls. Fig. 3 illustrates the spatial patterns along the first three pairs of canonical variates for the separately analyzed cohorts of HCs, asymptomatic LRRK2 pathogenic variant carriers and PD subjects. For HCs (Fig. 3a), DTBZ showed significant negative loadings for all dominant side regions for the first pair of canonical variates, which accounted for approximately 83 % of the variance; significant negative loadings for MP were detected for all regions except the caudate (both sides) and the non-dominant anterior putamen. For the second pair of canonical variates, DTBZ revealed significant negative loadings for all regions except the dominant middle and posterior putamen. MP only revealed significant negative loadings in the non-dominant middle putamen. The third pair of canonical variates showed significant negative loadings only for the dominant and non-dominant posterior putamen of DTBZ, whereas MP showed significant negative loadings in all regions. However, the second and third pair of canonical variates accounted for only ~10 % of the variance. Subject scores along the third pair of canonical variates (Fig. 4a, supplementary Table 3b) correlated significantly with age for MP ($p = 0.0004$). Note that the sign of the loadings are to be interpreted in the context of subject scores. With this in mind, the first two pairs of canonical variates mostly reflect fairly uniform variability across regions, independent of age, while the third pair of canonical variates for component 3 represents an-age dependent change in MP binding across all regions.

Asymptomatic LRRK2 pathogenic variant carriers. For the asymptomatic LRRK2 pathogenic variant carriers (Fig. 3b), both DTBZ and MP revealed significant negative loadings in all striatal regions for the first canonical pair (accounting for up to 95 % of the variance), whereas no significant loadings were detected for the second and third pair of canonical variates for either tracer. Subject scores along the first pair of canonical variates (Fig. 4b, supplementary Table 3b) correlated significantly with age for MP ($p = 0.003$). DTBZ subject scores revealed a similar trend ($p = 0.05$), reflecting an overall decline in binding as a function of age with a stronger emphasis on MP.

PD subjects. Spatial patterns of the PD cohort (Fig. 3c) showed significant negative loadings for all regions for DTBZ and MP for the first pair of canonical variates accounting for up to 89 % of the data. The spatial pattern along the second pair of canonical variates revealed a decreasing gradient in loadings from the caudate towards the posterior putamen with significant loadings for the less and more affected caudate, as well as the less affected anterior putamen for both tracers. The third pair of canonical variates of PD subjects demonstrated an asymmetrical pattern between the less and more affected sides for both tracers, however, loadings were not significantly different from zero.

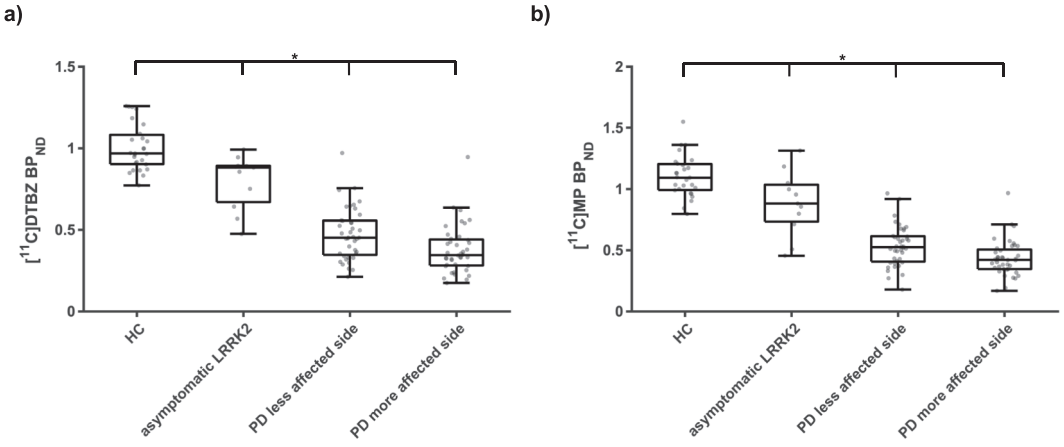

Fig. 1. Average DTBZ (a) and MP (b) BP_{ND} of the putamen for healthy controls (HC) and asymptomatic LRRK2 pathogenic variant carriers, and for the less and more affected side of the putamen for PD subjects. Note that the average BP_{ND} values are displayed for HCs and asymptomatic LRRK2 pathogenic variant carriers as no difference between the dominant and non-dominant putaminal BP_{ND} was detected for these subject cohorts. DTBZ = dihydrotetrabenazine; MP = methylphenidate; HC = healthy control; LRRK2 = leucine-rich repeat kinase 2; PD = Parkinson's Disease. * = $p < 0.05$ after Bonferroni-Holm's correction for multiple comparisons.

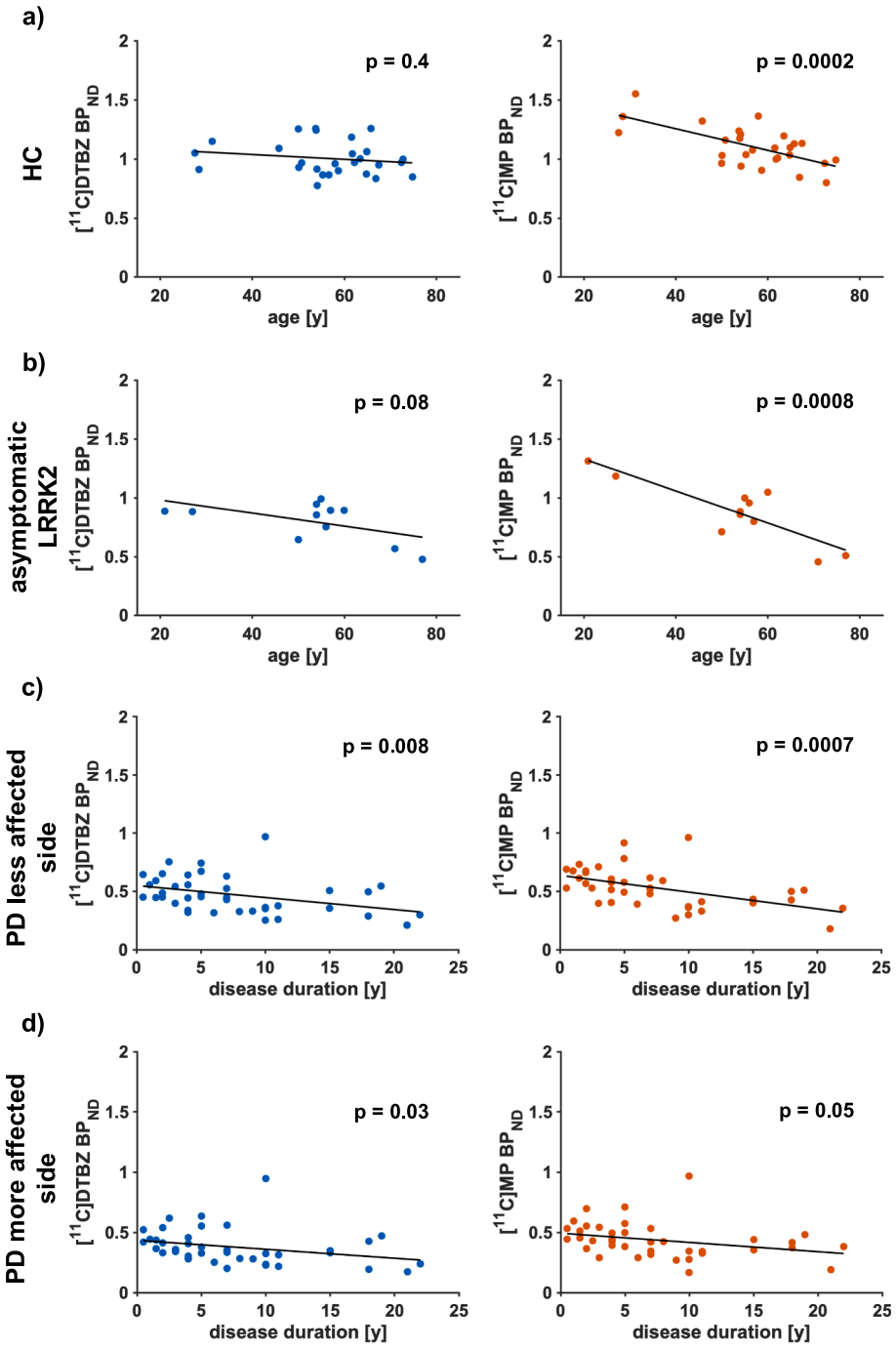

Fig. 2. DTBZ (left) and MP (right) BP_{ND} along age for the putaminal BP_{ND} averaged over both hemispheres for HCs (a) and asymptomatic LRRK2 pathogenic variant carriers (b), and along disease duration for the less affected (c) and more affected (d) sides of the putamen for PD subjects. Note that the average BP_{ND} values are displayed for HCs and asymptomatic LRRK2 pathogenic variant carriers as no difference between the dominant and non-dominant putaminal BP_{ND} was detected for these subject cohorts. DTBZ = dihydrotetrabenazine. MP = methylphenidate. HC = healthy control; LRRK2 = leucine-rich repeat kinase 2; PD = Parkinson's Disease.

The second and third pair of canonical variates accounted for ~ 10 % of the variance.

Subject scores along the first pair of canonical variates (Fig. 4c, supplementary Table 3) correlated significantly with disease duration as the sole significant explanatory variable (DTBZ: p = 0.03, MP: p = 0.008) illustrating that an overall decrease in binding – with some rostrocaudal gradient - is the most strongly expressed common disease-related feature for both DTBZ and MP.

3.2.2. *Pooled cohorts*

Combination of all three cohorts. The combination of all three cohorts (Fig. 5a) revealed significant negative loadings for all striatal regions and both tracers along the first pair of canonical variates (95 % of the variance), similar to the asymptomatic LRRK2 carriers and PD only spatial patterns (see Fig. 3b and c, respectively). The second pair of canonical variates revealed an asymmetric pattern between the less and more affected sides for each striatal region with significant loadings for the less affected caudate, anterior and middle putamen of DTBZ and MP.

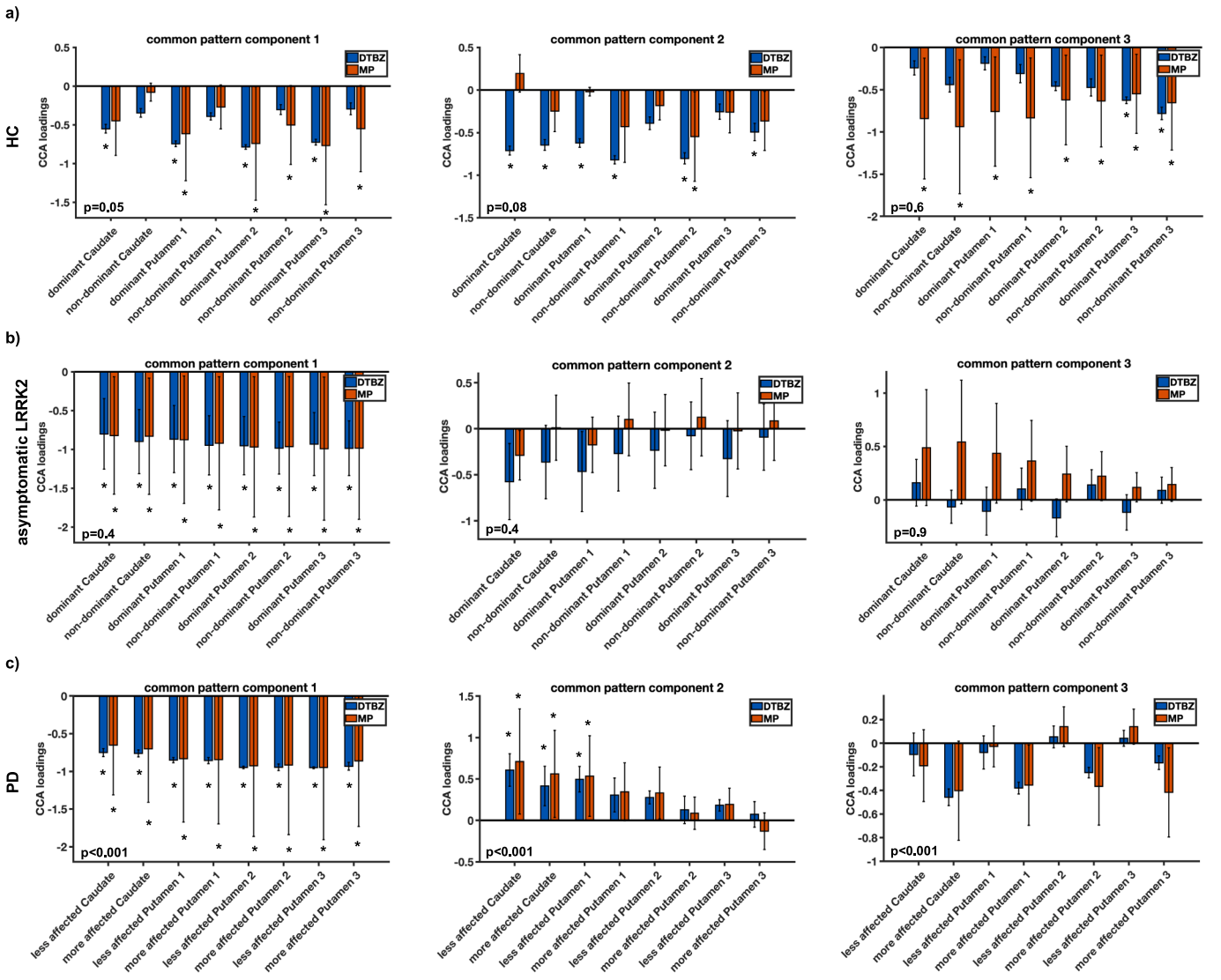

Fig. 3. Common spatial patterns along the canonical variates for DTBZ and MP for separate analyzed cohorts of HCs (a), asymptomatic LRRK2 pathogenic variant carriers and PD subjects (c). Number of canonical variates was set to three. Significant MCCA loadings ($p < 0.05$) are marked by an asterisk for the respective region. The Bonferroni-Holm method to correct for multiple testing was applied separately for each tracer and canonical variate. p-values of random permutation tests along each canonical variate are specified in the individual subgraphs. MCCA = multiset canonical correlation analysis. DTBZ = dihydrotetrabenazine. MP = methylphenidate. HC = healthy control; LRRK2 = leucine-rich repeat kinase 2. PD = Parkinson's Disease.

This asymmetric pattern is similar to the PD only pattern along the third pair of canonical variates (Fig. 3c). The spatial pattern along the third pair of canonical variates revealed a gradient of decreasing loadings from the caudate towards the posterior putamen for both tracers with significant DTBZ and MP loadings for the caudate (both sides) and significant loadings for the less affected anterior putamen for MP only. This pattern is similar to the second spatial pattern of PD only (Fig. 3c). However, second and third pair of canonical variate accounted for only up to 4 % of the variance.

Subject scores along the first pair of canonical variates of the three combined cohorts (Fig. 5b) revealed significant differentiation between all three cohorts for both tracers. A clear separation of subject scores between HCs (all subject scores were negative, which coupled with negative loadings, indicated higher than average BP_{ND} values) and PD subjects (all PD subjects scores except one - the previously noted outlier in univariate analysis - were positive) was detected along this canonical variate ($p < 0.0001$). Subject scores of the asymptomatic LRRK2 pathogenic variant carriers along this canonical variate revealed an increasing trend as a function of age from negative (HCs) towards positive subject scores (PD subjects) and were significantly different from HCs (DTBZ: $p < 0.0001$, MP: $p = 0.002$) and PD subjects scores (both tracers $p < 0.0001$). A positive correlation with age (Fig. 5b and supplementary Table 3b) was detected for the subject scores of MP for HCs ($p = 0.0002$). Subject scores along the first pair of canonical variates of the asymptomatic LRRK2 pathogenic variant carriers revealed a positive correlation with age for DTBZ and MP ($p = 0.04$ and $p = 0.002$, respectively, Fig. 5, supplementary Table 3a and b) and for MP along the second pair of canonical variates ($p = 0.02$). PD subjects scores along the second pair of canonical variates correlated significantly with disease duration as the sole significant explanatory variable for both DTBZ ($p = 0.02$, supplementary Table 3a) and MP ($p = 0.0005$, supplementary Table 3b). In addition, MP subject scores along the third pair of canonical variates for the PD group correlated significantly with age as a sole significant explanatory variable ($p = 0.03$, supplementary Table 3b).

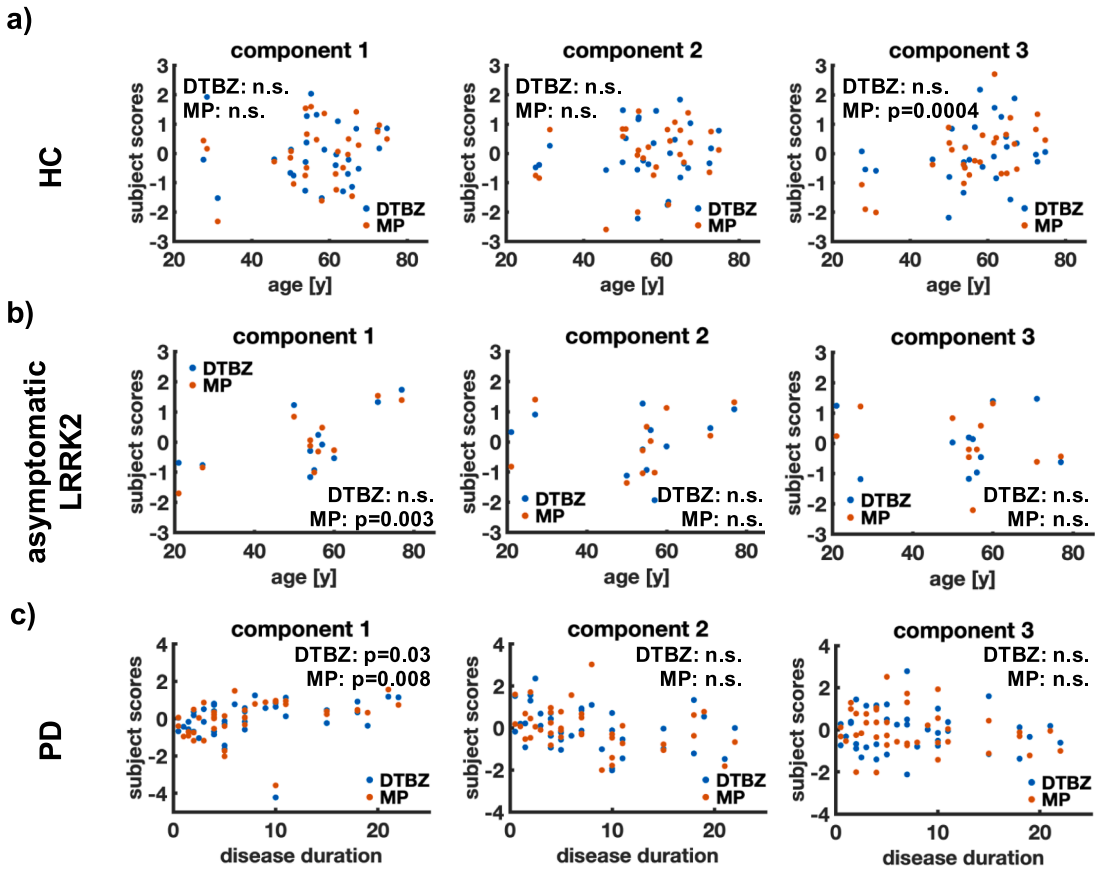

Fig. 4. Subject scores along age for HCs (a) and asymptomatic LRRK2 pathogenic variant carriers (b) and along disease duration for PD subjects (c) for both DTBZ and MP. Number of canonical variates was set to three pairs. Significant p-values using linear regression for HCs and asymptomatic LRRK2 pathogenic variant carriers, and multiple regression for PD subjects are specified. DTBZ = dihydrotetrabenazine. MP = methylphenidate. HC = healthy control; LRRK2 = leucine-rich repeat kinase 2.

4. Discussion

This study utilized a joint pattern analysis approach to identify spatial patterns for three different subject cohorts that underwent DTBZ and MP PET scans. PET scans were performed sequentially and were separated by at least 2.5 h to allow for tracer decay and to avoid any interferences. Spatial pattern were determined for separate and combined cohorts: (i) healthy controls, (ii) asymptomatic LRRK2 pathogenic variant carriers, (iii) PD subjects and (iv) all 3 cohorts pooled. The aim was to identify disease-specific spatial patterns over a wide range of disease durations (0.5–22 years) as previously done for early PD patients (disease duration 4.7 ± 2.8 years) (Fu, 2019) and to investigate the disease-specific patterns in relation to healthy control data. Furthermore, data from asymptomatic LRRK2 pathogenic variant carriers were included in the study in order to capture potential pre-symptomatic disease-induced patterns and/or genetic pathogenic variant-specific alterations in the dopaminergic system (Wile, 2017).

4.1. Univariate analysis

Results from the univariate analysis were found to be overall consistent with published data (Wile, 2017; Bohnen, 2006; Kaasinen and Vahlberg, 2017). Age-normalized analysis of asymptomatic LRRK2 pathogenic variant carriers and PD BP_{ND} values based on a previously published age correction method (Nandhagopal, 2008) to correct for age effects revealed comparable results (data not shown). We used a linear rather than exponential function (Nandhagopal, 2009; Nandhagopal, 2011) to describe the relation between the imaging data and age and disease duration, similar to other PET and SPECT studies (Kaasinen and Vahlberg, 2017).

4.2. Joint pattern analysis

4.2.1. Individual cohorts

Healthy controls. In HCs the joint pattern analyses demonstrated a trend towards an asymmetrical pattern between dominant and non-dominant striatal regions for DTBZ and MP. Only right-handed subjects were included in our healthy control cohort and univariate statistical testing with correction for multiple testing demonstrated no significant differences in BP_{ND} between the dominant and non-dominant striatal sides along with an asymmetry index below 10 % (see Table 1). The presence of asymmetric lateralization in HCs has been a source of debate over the last decades with studies presenting contradictory results. In a recent study, Garrido et al. determined symmetric dopaminergic functions using DAT-SPECT (Garrido, 2020), whereas several studies provide evidence of lateralization (Larisch, 1998; Vernaleken, 2007). Given the previously reported higher sensitivity of MCCA to topological differences compared to univariate analysis (Fu, 2019), we conclude that MCCA may have been better able to capture the asymmetrical pattern in striatal regions of HCs than the univariate analysis.

Spatial patterns along the third pair of canonical variates revealed significant negative loadings in all striatal regions only for MP together with a significant correlation between subject scores and age (Fig. 3a and 4a), demonstrating - similar to the univariate analysis - the dependency of BP_{ND} with age (Wile, 2017; Adams, 2005; Kish, 1992). The fact that predominantly the MP- and not the DTBZ -related loadings were significant is consistent with the fact that age dependence was only observed for MP and not DTBZ. Interestingly, the second canonical

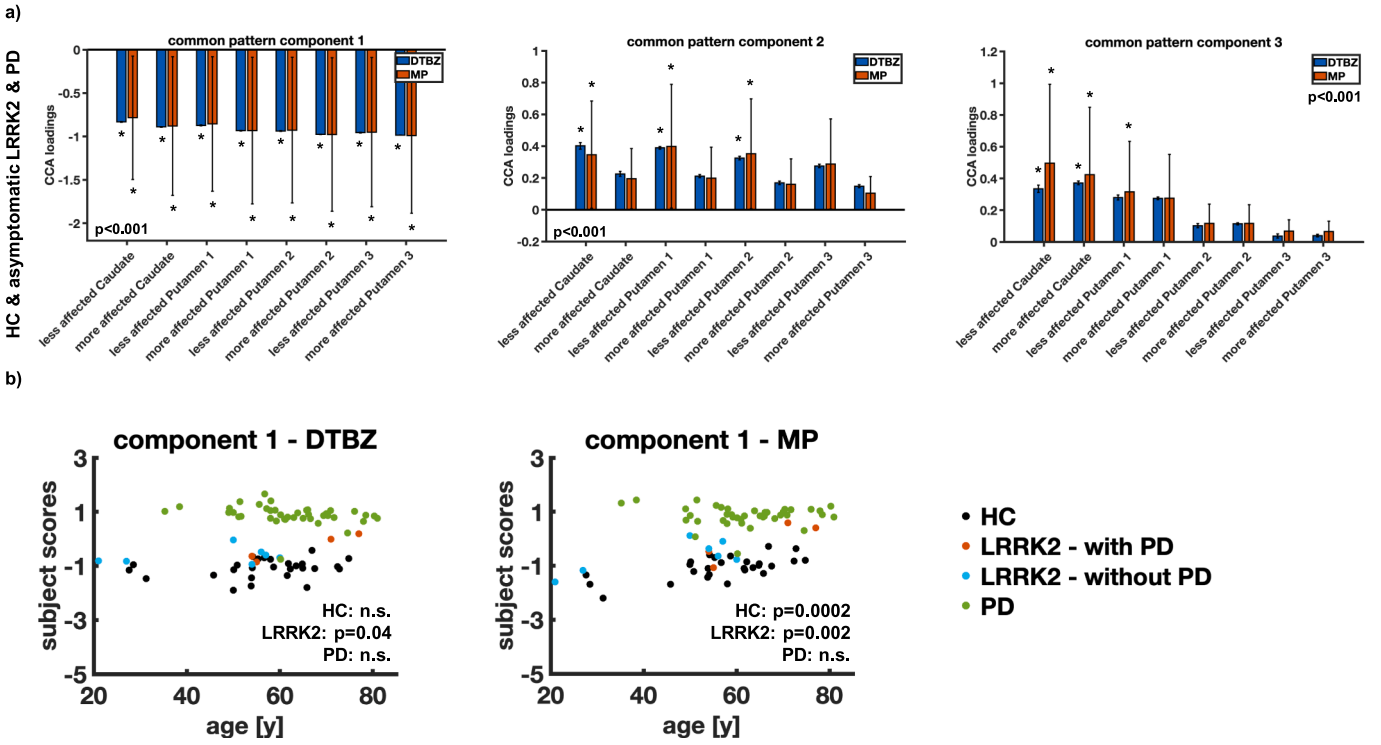

Fig. 5. Common spatial patterns (a) along the canonical variates for DTBZ and MP for pooled cohorts of HCs, asymptomatic LRRK2 pathogenic variant carriers and PD subjects and corresponding subject scores (b) along age for the first canonical variate. Note that asymptomatic LRRK2 pathogenic variant carriers are classified based on the clinical follow-up data. Number of canonical variates was set to three pairs to determine common spatial patterns. Significant CCA loadings ($p < 0.05$) are marked by an asterisk for the respective region. The Bonferroni-Holm method to correct for multiple testing was applied separately for each tracer and canonical variate. p-values of random permutation tests along each canonical variate are specified in the individual subgraphs. Note that when the HC and/or the LRKK2 subjects' data are pooled with the PD group, we distinguish between the less affected and more affected striatal regions for the PD cohort and use the average BP_{ND} values between the dominant and non-dominant side for the HC and LRRK2 pathogenic variant carriers. Left column of the subjects scores displays all subject scores along age for pooled cohorts for DTBZ; right column displays subject scores along age for pooled cohorts for MP. Significant p-values using linear regression for HCs and asymptomatic LRRK2 pathogenic variant carriers, and multiple regression for PD subjects are specified. CCA = canonical correlation analysis. DTBZ = dihydrotetrabenazine. MP = methylphenidate. HC = healthy control; LRRK2 = leucine-rich repeat kinase 2; PD = Parkinson's Disease.

variate mainly shows significant loadings arising from DTBZ data but no correlation of subject scores with age was found, implying relative changes in VMAT2 and DAT may be due to different underlying mechanisms.

Asymptomatic LRRK2 pathogenic variant carriers. The spatial pattern for the first canonical pair of variates of the asymptomatic LRRK2 pathogenic variant carriers (Fig. 3b) revealed a pattern similar to that of PD patients (Fig. 3c) compatible with the dominant common pattern representing an overall loss of dopaminergic terminals in striatal regions. Subject scores of MP correlated with age for this canonical variate, likely reflective of the increased risk of disease in carriers of pathogenic LRRK2 variants with increasing age (Wile, 2017), but less sensitive compared to univariate analysis. However, the spatial patterns along component 1 for asymptomatic LRRK2 pathogenic variant carriers are a result of both age-related decline of MP (seen also in HCs) and incipient PD. The univariate analysis is less likely to separate the two effects. DTBZ subject scores of this canonical variate revealed a similar trend as a function of age ($p = 0.05$) possibly indicating preclinical disease with increased age, given that no age dependence was observed for DTBZ patterns in the HC group. No asymmetrical patterns between dominant and non-dominant sides were detected for this component in contrast to component 1 of HCs. This could have some potential physiological explanation, however, we believe that it is may more likely due to the fact that the difference is small even in HCs and the number of LRRK2 pathogenic variant carriers is limited in this study.

Spatial patterns of the second canonical variate revealed an asymmetry between the dominant and non-dominant striatal regions for the LRRK2 pathogenic variant carriers, similar to the first canonical variate of the HCs, however the loadings were not statistically significant, potentially indicating less 'physiologic' asymmetry in incipient disease, but also potentially arising from the smaller sample size in the asymptomatic LRRK2 group.

The third canonical variate revealed the rostro-caudal gradient pattern primarily for MP. Here, loadings were not statistically significant, in contrast to the second canonical variate of the PD only pattern, thus possibly revealing a trend toward this disease-induced pattern in this subject cohort.

PD subjects. The spatial pattern of PD subjects along the first pair of canonical variates represents the overall loss of dopaminergic terminals with significant negative loadings in all investigated striatal regions (Fig. 3c). Subject scores of this canonical variate (Fig. 4c) correlated significantly with disease duration for DTBZ and MP ($p = 0.03$ and $p = 0.008$, respectively), similar to univariate analysis (less affected side: DTBZ: $p = 0.008$, MP: $p = 0.0007$; more affected side: DTBZ: $p = 0.03$, MP: n.s.). Similar to the univariate analysis, subject scores of one subject along the first pair of canonical variates appeared as an outlier. Removing this subject from the analysis revealed a stronger correlation of disease duration with subject scores both for DTBZ ($p = 0.002$) and MP ($p < 0.0001$), as well as a correlation with age (DTBZ: $p = 0.006$, MP: $p = 0.01$) for the first canonical variate. Interestingly, similar to the subject score correlation with age, when this outlier was removed from the univariate analysis, a correlation of the DTBZ BP_{ND} values with age was detected for both putaminal sides for DTBZ with a stronger correlation for the more affected side (less affected side: $p = 0.048$, more affected side: $p = 0.02$).

A previous study determined a similar overall loss of dopaminergic

neurons in an early PD patient cohort (4.7 ± 2.8 years), as well as a correlation of subject scores with disease duration both for DTBZ and MP (Fu, 2019), similar to our results. The disease duration of subjects enrolled in the present study spanned a larger range (7.5 ± 5.9 years) hence resulted in a more heterogeneous patient cohort compared to the previous study in whom more rapid dopaminergic changes may be present. Those subjects with moderate to advanced disease will contribute particularly strongly to the spatial pattern of the progressive loss, as they have a more profound loss of neurons compared to early PD subjects.

The impact of the more heterogeneous patient cohort spanning a wider range of disease durations is also demonstrated by the fact that in the present study the first pair of canonical variates (i.e. spatial patterns associated with the strongest correlation between DTBZ and MP) revealed the overall loss of dopaminergic neurons demonstrating the strongest impact of this disease-specific pattern, whereas in the study by Fu et al. focusing on an early PD patient cohort the third pair of canonical variates revealed this pattern (Fu, 2019).

The spatial pattern of PD subjects along the second pair of canonical variates (Fig. 3c) revealed the anterior to posterior gradient with highest loadings in the caudate and decreasing loadings towards the posterior putamen. Importantly, this gradient is not the result of partial volume effects (PVEs) inherently present in PET imaging, which can result in lower measured PET uptake in smaller regions due to spill-over of the activity signal (Soret et al., 2007), hence lower signal in the posterior putamen compared to the caudate and anterior putamen. However, as this gradient was not present in spatial patterns of HCs (Fig. 3a), in which the PVE is also present, the gradient detected for PD subjects is a disease-related specific pattern, in keeping with the well-known rostrocaudal gradient of dopamine denervation in PD subjects (Antony, 2013).

The third pair of canonical variates revealed the disease-induced asymmetric pattern between the more and less affected striatal regions (Fig. 3c), which is known to be an early-disease induced pattern (Nandhagopal, 2009). Comparing these results to the results by Fu et al. (Fu, 2019), for which the asymmetric pattern had the strongest influence in the pattern analysis due to the shorter disease duration, this underlies the fact that the asymmetrical pattern in PD subjects with long disease duration is less distinct. This has also been reported by Nandhagopal et al. (Nandhagopal, 2009).

4.2.2. Pooled cohorts

Combination of all three cohorts. The combination of all three cohorts revealed all three disease-related patterns (Fig. 5a), consistent with previous findings, with highly significant loadings for the first canonical variate, underlying the strong impact of the overall loss of dopaminergic terminals. The loadings of this canonical variate demonstrated a more robust level of significance compared to loadings of PD subjects only, revealing an amplification of the pattern when HCs are used as reference. The first pair of canonical variates, which in this case reflects the overall loss of dopaminergic terminals for the PD group, provides the most common information between the two tracers; however, no significant correlation of subject scores with disease duration was found, possibly consistent with the fact that an overall decrease was already observed in the asymptomatic pathogenic variant carrier group and could be a manifestation of disease presence rather than progression, whose impact may be masked by floor effects. Once the effect of the overall magnitude is removed, the second pair of canonical variates is associated with disease progression in the PD group (asymmetrical pattern with significant loadings for the less affected caudate and anterior and middle putamen, respectively) for both DTBZ and MP. This finding is in line with results from a previous study focusing on early PD subjects demonstrating that the uptake in the less affected side might provide a more sensitive marker of disease progression compared to the more affected side (Fu, 2019). Interestingly, the second canonical variate also shows a significant age dependence for the asymptomatic LRRK2 group for MP, again indicating either incipient disease or that alterations in DAT may be selective risk factors for disease.

The spatial patterns obtained with the pooled groups appeared to be driven primarily by the PD group and can thus be taken to be reflective of disease-related alterations; subject scores obtained from the pooled patient cohorts show a clear separation of the three subject groups. For the first canonical variate, the subject scores of the asymptomatic LRRK2 pathogenic variant carriers become closer to those of the PD subjects for both MP and DTBZ with increasing age, indicating an increasingly PD-like alteration of the dopaminergic terminals, reflective of the increased risk of asymptomatic LRRK2 pathogenic variant carriers to develop PD as they age (Fig. 5b). For this canonical variate even the subject scores of the HCs for MP increase with age, possibly reflecting the fact that age itself is a risk factor for PD. It's known that there is an age-related decrease in MP binding (Kish, 1992; Troiano, 2010), but the pattern detected here is different from the one observed in healthy aging, where the loss is more uniform across the striatum. Although not significantly different, the slope appears steeper for the LRRK2 cohort (HC: $R^2 = 0.42$, asymptomatic LRRK2: $R^2 = 0.66$, $p = 0.2$), consistent with the additional pathogenic variant-related risk factor for PD. Additionally, given the similarity of the patterns obtained in the pooled cohorts and those observed in the asymptomatic LRRK2 cohort, it seems very unlikely that the asymptomatic LRRK2 cohort patterns would be indicative of compensatory changes, but they are more likely to reflect incipient disease or risk of disease. This is consistent with literature where early compensatory change in this subject population has been identified in the serotonergic but not dopaminergic system (Wile, 2017; Fu, 2021). Furthermore, clinical follow-up of this patient cohort revealed that out of the 11 subjects included in this study 4 subjects were later diagnosed with PD, whereas 7 subjects reported no manifestation of PD. Two subjects that revealed subject scores closest to PD subjects were among those diagnosed with PD. This amplifies our hypothesis that the determined LRRK2 patterns reflect pre-manifestation of disease.

The PD subject that appeared as outlier both in univariate analysis, as well as in subject scores of PD subjects only, reveals subject scores similar to HCs and asymptomatic LRRK2 pathogenic variant carriers when patient cohorts are pooled. The clinical characteristics of the subject did not differ from other PD subjects (Hoehn and Yahr scale of 1.5); the subject can be classified as a 'scan without evidence of

Table 2
Correlation strength (R^2) between subject scores of DTBZ and MP and p-values of random permutation tests along each canonical variate. HC = healthy control; LRRK2 = leucine-rich repeat kinase 2; PD = Parkinson's Disease.

subject cohort	canonical variate 1		canonical variate 2		canonical variate 3	
	R^2	p-value	R^2	p-value	R^2	p-value
HC	0.44	0.05	0.15	0.08	<0.01	0.6
asymptomatic LRRK2 pathogenic variant carriers	0.68	0.4	0.28	0.4	<0.01	0.9
PD	0.76	**<0.001**	0.42	**<0.001**	0.35	**<0.001**
HC pooled with asymptomatic LRRK2 pathogenic variant carriers	0.55	**<0.001**	0.28	**<0.001**	<0.01	0.6
HC pooled with PD	0.90	**<0.001**	0.45	**<0.001**	0.16	**<0.001**
asymptomatic LRRK2 pathogenic variant carriers pooled with PD	0.84	**<0.001**	0.54	**<0.001**	0.31	**<0.001**
HC pooled with asymptomatic LRRK2 pathogenic variant carriers and PD	0.89	**<0.001**	0.49	**<0.001**	0.16	**<0.001**

dopaminergic deficit' (SWEDD) (Batla, 2014; Wile, 2016). Longitudinal follow-up PET scans were not performed, however clinical follow-up of this subject revealed a mild and indolent onset of PD.

As expected, the analysis of the combined cohorts revealed a statistically more robust separation between patient groups compared to the univariate analysis, confirming that MCCA is more sensitive to disease-related abnormalities compared to traditional univariate analysis. An additional advantage is the fact that compared to the regional univariate analysis MCCA suffers less from the multiple comparison problem.

4.3. Correlation strength for each pair of canonical variates

The correlation strength (R^2) between each set of canonical variates and the p-values of random permutation tests along each canonical variate are shown in Table 2. The correlation strength between MP and DTBZ patterns increases from health to disease, supporting evidence that such correlations are disease-related. This is not entirely surprising as MP and DTBZ are both indirect and macroscopic markers of presynaptic terminal density, the main macroscopic dopaminergic feature affected in PD. The correlation strength between common patterns is higher in the asymptomatic LRRK2 pathogenic variant carriers compared to the control group, possibly reflective of pre-symptomatic disease, however p-values of HCs were stronger compared to asymptomatic LRRK2 pathogenic variant carriers likely due to the smaller sample size of the asymptomatic LRRK2 cohort and the likely more heterogeneous state of the pathogenic variant carriers. Furthermore, except for when HC alone are considered, the first canonical variate always reflects an overall decrease of tracer uptake, indicating that the most important common feature between DTBZ and MP likely just reflects dopaminergic terminal loss in both PD and asymptomatic LRRK2 subjects. The second canonical variate is in all cases related to the asymmetry between sides with significant loadings for the pooled cohorts, with the exception of the HC and PD only cases; note however that in the PD-only case the asymmetry is captured by the third canonical variate, which has a correlation coefficient of 0.35 vs. 0.42 for the second canonical variate. Since the correlation strengths are comparable, the ordering of second and third canonical variates is very similar. This finding implies that the second most important common alteration is the asymmetric uptake in the less and more affected sides of the striatum. The third canonical variate is consistently associated with the rostro-caudal gradient (with significant loadings for the pooled cohorts) with the same exceptions as above.

4.4. Limitations

The data analyzed in this study were acquired using the ECAT 953B/31 scanner (Siemens), a relatively low resolution PET scanner compared to current state-of-the-art systems (Sossi, 1998). We did however use an optimized data processing pipeline to ensure good co-registration of the images and good accuracy of ROI placement. In direct comparison with the results by Fu et al., MCCA results of the first canonical variate revealed the overall dopaminergic loss, which was not detected by Fu et al. due to the shorter disease duration analyzed (Fu, 2019). The second canonical variate was consistent between both studies representing the anterior to posterior gradient. The third canonical variate representing the disease-related asymmetry is less prominent in this study, whereas the patient cohort analyzed in Fu et al. revealed the asymmetrical pattern for component 1 demonstrating the strongest impact. These differences might be due to the facts that (i) the data for the study by Fu et al. were acquired on a much higher resolution scanner, the high-resolution research tomograph (HRRT, Siemens), (resolution ~ $(2.0\ mm)^3$) compared to the data acquired on the ECAT system and (ii) the disease duration analyzed in the present study spans a much larger range compared to Fu et al. and thus includes later times when the PET measures approach a plateau.

Another possible limitation is the fact that the number of asymptomatic LRRK2 pathogenic variant carriers (n = 11) included in this study is relatively low compared to healthy controls (n = 27) and PD subjects (n = 40); however, we speculate that the 11 subjects analyzed in this study are a reasonable representation of a larger cohort as our univariate analysis results are consistent with literature.

Alterations observed in the asymptomatic LRRK2 pathogenic variant carriers group could, in principle, reflect compensatory changes rather than direct effects of pre-symptomatic disease. Compensatory changes have been investigated previously showing that a high loss of neurons can be compensated by overexpression of synthesis and release of the remaining neurons (Adams, 2005; Lee, 2000). However, as pooled MCCA results of all three cohorts revealed increased loss of DTBZ uptake with age in asymptomatic LRRK2 pathogenic variant carriers along the first canonical variate, as well as similar patterns for the asymptomatic LRRK2 cohort compared to the pooled cohorts, we deem the detected changes in our study more consistent with pre-symptomatic disease-induced effects, in line with literature that showed compensatory changes for this cohort to be more evident in the serotonergic rather than the dopaminergic system (Wile, 2017; Fu, 2021).

We did not apply corrections for multiple comparisons when we evaluated metrics' dependence on age due to a still relatively limited number of subjects for such an extended analysis; hence, significance of these results needs to be interpreted with some degree of caution.

And finally, we did not include LRRK2 pathogenic variant carriers in the analysis although they would provide a cleaner comparative group for the asymptomatic LRRK2 pathogenic variant carriers as we did not have a large enough group for such a comparison. Previous studies however repeatedly reported indistinguishable degeneration of the dopaminergic system between sporadic and LRRK2-associated PD (Wile, 2017; Adams, 2005).

5. Conclusion

Using an entirely data driven approach and images obtained from two dopaminergic pre-synaptic markers, we identified PD-induced spatial distribution alterations common to DAT and VMAT2 in both asymptomatic LRRK2 pathogenic variant carriers and PD subjects. The inclusion of HCs in the analysis demonstrated that the dominant common PD-induced pattern is related to an overall dopaminergic terminal density denervation, followed by asymmetry and rostro-caudal gradient with deficits in the less affected side still being the best marker of disease progression. The approach revealed an increasing correlation between MP and DTBZ spatial pattern transitioning from the HC to the PD group, highlighting disease-induced common effects on DAT and VMAT2. Subject scores from the combined analysis yielded a stronger separation between patient cohorts compared to univariate analysis, confirming that MCCA is more sensitive to disease effects compared to traditional univariate analysis and may hence provide more insights into disease-specific processes. The analysis was indeed able to capture a trend towards PD-related patterns in the LRRK2 pathogenic variant carrier cohort with increasing age in line with the known increased risk of this patient cohort to develop PD as they age. The advantage of this method thus resides in its ability to identify not only regional differences in tracer binding between groups, but also common disease-related alterations in the spatial distribution patterns of tracer binding, thus potentially capturing more complex aspects of disease induced alterations. While in this case common alterations between DTBZ and MP binding were expected, being both presynaptic dopaminergic markers, the method can be applied to other multi-modal studies to evaluate impact of disease on more complex brain processes.

CRediT authorship contribution statement

Julia G. Mannheim: Data curation, Investigation, Validation, Visualization, Writing – original draft, Writing – review & editing, Formal analysis, Methodology. **Jessie Fanglu Fu:** Writing – review &

editing, Conceptualization, Data curation, Investigation, Methodology, Software. **Tilman Wegener:** Formal analysis, Software, Writing – review & editing, Data curation. **Ivan S. Klyuzhin:** Data curation, Software, Writing – review & editing. **Nasim Vafai:** Data curation, Software, Writing – review & editing. **Elham Shahinfard:** Data curation, Resources, Writing – review & editing. **Jessamyn McKenzie:** Data curation, Resources, Writing – review & editing. **Audrey Strongosky:** Data curation, Writing – review & editing. **Zbigniew K. Wszolek:** Data curation, Writing – review & editing. **A. Jon Stoessl:** Project administration, Resources, Conceptualization, Supervision, Validation, Writing – review & editing. **Vesna Sossi:** Conceptualization, Project administration, Supervision, Writing – review & editing, Resources, Validation.

Declaration of Competing Interest

The authors declare that they have no known competing financial interests or personal relationships that could have appeared to influence the work reported in this paper.

Data availability

The data that has been used is confidential.

Acknowledgements

We would like to express our sincere gratitude to all subject volunteers for their support. Furthermore, we would like to thank the UBC PET scanning team, as well as the TRIUMF radiochemistry production team. This study was partially funded through Natural Sciences and Engineering Research Council grant (240670-13).

Appendix A. Supplementary data

Supplementary data to this article can be found online at https://doi.org/10.1016/j.nicl.2024.103600.

References

Adams, J.R., et al., 2005. PET in LRRK2 mutations: comparison to sporadic Parkinson's disease and evidence for presymptomatic compensation. Brain 128 (Pt 12), 2777–2785.
Antony, P.M., et al., 2013. The hallmarks of Parkinson's disease. FEBS J. 280 (23), 5981–5993.
Batla, A., et al., 2014. Patients with scans without evidence of dopaminergic deficit: a long-term follow-up study. Mov. Disord. 29 (14), 1820–1825.
Bohnen, N.I., et al., 2006. Positron emission tomography of monoaminergic vesicular binding in aging and Parkinson disease. J. Cereb. Blood Flow Metab. 26 (9), 1198–1212.
Fu, J.F., et al., 2019. Joint pattern analysis applied to PET DAT and VMAT2 imaging reveals new insights into Parkinson's disease induced presynaptic alterations. Neuroimage Clin 23, 101856.
Fu, J.F., et al., 2021. Serotonergic system impacts levodopa response in Early Parkinson's and future risk of dyskinesia. Mov. Disord. 36 (2), 389–397.
Garrido, A., et al., 2020. Lack of Asymmetry of nigrostriatal dopaminergic function in healthy subjects. Mov. Disord. 35 (6), 1072–1076.
Kaasinen, V., Vahlberg, T., 2017. Striatal dopamine in Parkinson disease: a meta-analysis of imaging studies. Ann. Neurol. 82 (6), 873–882.
Kish, S.J., et al., 1992. Aging produces a specific pattern of striatal dopamine loss: implications for the etiology of idiopathic Parkinson's disease. J. Neurochem. 58 (2), 642–648.
Larisch, R., et al., 1998. Left-right asymmetry of striatal dopamine D2 receptors. Nucl. Med. Commun. 19 (8), 781–787.
Lee, C.S., et al., 2000. In vivo positron emission tomographic evidence for compensatory changes in presynaptic dopaminergic nerve terminals in Parkinson's disease. Ann. Neurol. 47 (4), 493–503.
Nandhagopal, R., et al., 2008. Progression of dopaminergic dysfunction in a LRRK2 kindred: a multitracer PET study. Neurology 71 (22), 1790–1795.
Nandhagopal, R., et al., 2009. Longitudinal progression of sporadic Parkinson's disease: a multi-tracer positron emission tomography study. Brain 132 (Pt 11), 2970–2979.
Nandhagopal, R., et al., 2011. Longitudinal evolution of compensatory changes in striatal dopamine processing in Parkinson's disease. Brain 134 (Pt 11), 3290–3298.
Peng, S., et al., 2013. Dopamine: PET imaging and Parkinson disease. PET Clin 8 (4), 469–485.
Rui, Q., et al., 2018. The role of LRRK2 in neurodegeneration of Parkinson disease. Curr. Neuropharmacol. 16 (9), 1348–1357.
Soret, M., Bacharach, S.L., Buvat, I., 2007. Partial-volume effect in PET tumor imaging. J. Nucl. Med. 48 (6), 932–945.
Sossi, V., et al., 1998. Quantitative comparison of three- and two-dimensional PET with human brain studies. J. Nucl. Med. 39 (10), 1714–1719.
Sossi, V., et al., 2010. Dopamine turnover increases in asymptomatic LRRK2 mutations carriers. Mov. Disord. 25 (16), 2717–2723.
Stoessl, A.J., 2011. Neuroimaging in Parkinson's disease. Neurotherapeutics 8 (1), 72–81.
Taymans, J.-M., Greggio, E., 2016. LRRK2 kinase inhibition as a therapeutic strategy for Parkinson's disease, where do we stand? Curr. Neuropharmacol. 14 (3), 214–225.
Tolosa, E., et al., 2020. LRRK2 in Parkinson disease: challenges of clinical trials. Nat. Rev. Neurol. 16 (2), 97–107.
Troiano, A.R., et al., 2010. Dopamine transporter PET in normal aging: dopamine transporter decline and its possible role in preservation of motor function. Synapse 64 (2), 146–151.
Vernaleken, I., et al., 2007. Asymmetry in dopamine D(2/3) receptors of caudate nucleus is lost with age. Neuroimage 34 (3), 870–878.
Wile, D.J., et al., 2016. A scan without evidence is not evidence of absence: scans without evidence of dopaminergic deficit in a symptomatic leucine-rich repeat kinase 2 mutation carrier. Mov. Disord. 31 (3), 405–409.
Wile, D.J., et al., 2017. Serotonin and dopamine transporter PET changes in the premotor phase of LRRK2 parkinsonism: cross-sectional studies. Lancet Neurol. 16 (5), 351–359.
Wu, Y., Carson, R.E., 2002. Noise reduction in the simplified reference tissue model for neuroreceptor functional imaging. J. Cereb. Blood Flow Metab. 22 (12), 1440–1452.
Zijlmans, J., et al., 2007. [123I] FP-CIT spect study in vascular parkinsonism and Parkinson's disease. Mov. Disord. 22 (9), 1278–1285.